Desalination and Water Treatment
www.deswater.com

doi: 10.5004/dwt.2021.27393

229 (2021) 206–216
July

Modification of conventional coagulation–flocculation process with graphene oxide and magnetite nanoparticles for turbidity removal from surface water

Shima Mardani, Vahid Aghabalaei, Mahla Tabeshnia, Majid Baghdadi*

School of Environment, College of Engineering, University of Tehran, Tehran, Iran, P.O. Box: 1417853111, Tel. +98 21 61113171; Fax: +98 21 66407719; emails: m.baghdadi@ut.ac.ir (M. Baghdadi), mardani.sh@ut.ac.ir (Sh. Mardani), aghabalaeivahid@ut.ac.ir (V. Aghabalaei), mahlatabeshnia@ut.ac.ir (M. Tabeshnia)

Received 23 November 2020; Accepted 6 May 2021

ABSTRACT

It is important to reduce the turbidity of drinking water to the level specified in the standards. Herein, conventional and modified coagulation–flocculation processes were applied to remove turbidity from drinking water. At first, the response surface methodology was utilized to design experiments, evaluate the effect of independent variables, and optimize the conventional coagulation process. According to the results of the analysis of variance, the maximum turbidity reduction of 95.7% was obtained under the optimal pH value of 6.9, $FeCl_3$ dosage of 48 mg/L, and mixing time of 46 s in the rapid mixing unit. After determining the optimal conditions of the conventional coagulation–flocculation process (CFP), to reduce the amount of turbidity according to the existing standards (5 NTU) for drinking water, the modified CFP with graphene oxide (GO) and magnetic (Fe_3O_4) nanoparticles was used. The highest efficiency of turbidity removal (97.6%) was achieved when a combination of GO and Fe_3O_4 was used, resulting in meeting the standard level of turbidity. On the other hand, the settling time was significantly reduced.

Keywords: Coagulation–flocculation process; Graphene oxide; Magnetic nanoparticles; Response surface methodology; Turbidity; Surface water

1. Introduction

World population growth, rising living standards, urban, industrial, and agricultural developments have caused increasing water consumption [1]. Mostly, surface water resources for drinking water have a high level of turbidity which has many undesired effects such as the sticking of microorganisms to particles, the sheltering viruses and cysts, and disinfection interference in the water purification processes. Additionally, many researchers have related digestive system disease to the high level of turbidity in the treated waters [2,3]. The desirable and allowable maximum limit of turbidity is 1 and 5 NTU, respectively, according to standard (No, 1053) specified by the Institute of Standards and Industrial Research of Iran (ISIRI) [4].

The coagulation–flocculation process (CFP) is widely used to remove the turbidity from drinking water. This technique can be classified into conventional and advanced (or modified) CFP [5,6]. In recent years, extensive researches have been conducted on the conventional CFP for turbidity removal with various coagulants [7–9], and the effect of different factors including the amount of different coagulants, velocity gradient, settling time, and camp number [10,11]. Although conventional CFP has been used for removing turbidity, in some cases, this process is not useful for turbidity reduction to less than 5 NTU, especially for the high turbidity waters. For example, studies by Kalavathy et al. [11] and Usefi and Ghalhari [12] showed that the effluent turbidity was not sufficient to meet the turbidity standard (5 NTU) for drinking water. An alternative to reduce further turbidity is the use of nanomaterials

* Corresponding author.

(modified CFP) in the water purification process due to their larger specific surface area and more functionalized sites [13].

Although nanoparticles including carbon-based nanostructured materials (CNMs), that is, graphene oxide (GO) and magnetite (Fe_3O_4) are widely employed for water purification [14–17], only a few studies have been published on the effects of GO and magnetic nanoparticles, separately or in combination for removing turbidity of high turbidity water by modified CFP [18–20]. For example, magnetic separation not only does the settling time decrease but also reduces the sludge volume and the operating costs [18,21]. Also, the oxygenated functional groups of GO help to improve the dispersing ability of GO and remove pollutants from water [22]. However, the aim of this study is optimization and verification of the CFP for removing turbidity of high turbidity water using the response surface methodology (RSM). The modified CFP was conducted under optimal conditions to investigate the effect of GO separately and in combination with Fe_3O_4 to provide the turbidity of less than 5 NTU.

2. Materials and methods

2.1. Materials

HCl and NaOH were obtained from Merck (Darmstadt, Germany), and also ferric chloride ($FeCl_3{\cdot}6H_2O$) was purchased from Sigma-Aldrich (St. Louis. MO). Zeolite as a turbidity source was prepared by Kimia Pars Shayankar Co., (Iran). Graphene oxide and magnetic nanoparticles were synthesized by Hummer and precipitation methods, respectively. Briefly, GO was prepared according to the Hummer method by adding 11.88 g of potassium nitrate to 500 mL of sulfuric acid at low temperatures. After that, it was mixed with 10 g of graphite powder and 60 g $KMnO_4$, respectively, and then 20 ml of H_2O_2 was added drop by drop at a low temperature. In order to remove impurity and ions that existed in produced precipitation, HCl (5% v/v) was used. Finally, the GO was obtained by sonication and drying at room temperature [23]. Also, magnetite nanoparticles were made using a precipitation method by adding 2.92 g of $FeCl_3{\cdot}6H_2O$ and 1.05 g of $FeCl_2{\cdot}4H_2O$ to 300 mL of deoxygenated water, prepared by purging nitrogen gas into deionization water. Then this compound was stirred by adding the 80 mL of NH_3 dropwise to the solution to get nanoparticles of Fe_3O_4 [24].

2.2. Preparation of sample waters

In this study, for coagulation tests, turbid water was prepared by adding 25 g of zeolite to 10 L of tap water. For achieving uniform dispersion of zeolite particles, the suspension was stirred for 1 h. Additionally, it was allowed to remain for 24 h for completing hydration of the particles, and it was used as the stock suspension. The turbidity of prepared water was 191 NTU.

2.3. Coagulation–flocculation experiments

Coagulation–flocculation experiments were done using a jar-test apparatus. The pH of zeolite suspension was adjusted using solutions of 0.1 mol/L of HCl and 0.1 mol/L of NaOH, and also ferric chloride was used as the coagulant. The CFP was consisting of a rapid mixing step (120 rpm) and a slow mixing step (30 rpm) followed by settling at room temperature (25°C ± 2°C). After 30 min of sedimentation, the upper clarified liquid was collected and residual turbidity was measured.

After determining the optimal operating conditions of conventional CFP using the design expert software, the performance of GO, and the combination of GO and Fe_3O_4 were examined to evaluate the efficiency of modified CFP for turbidity removal and the settling rate.

In the modified CFP with GO, firstly, 10 mg/L of GO and then 48 mg/L of $FeCl_3$ were added to the synthesized water with a pH of 6.9. Then it was mixed for approximately 46 s at high speed. Also, for the modified CFP with a combination of GO and Fe_3O_4, firstly 4 mg/L of Fe_3O_4 and 10 mg/L of GO were added and after homogenization, 48 mg/L of $FeCl_3$ was added. This process was consisting of a rapid mixing step (120 rpm) and a slow mixing step (30 rpm) followed by settling at room temperature (25°C ± 2°C).

2.4. Characterization of Fe_3O_4 and GO

To identify the morphology of GO and Fe_3O_4, scanning electron microscopy (SEM, Bruker, Germany) was applied. Furthermore, information about the structure of GO and Fe_3O_4 was obtained by an X-ray diffraction instrument using Cu Kα radiation (XRD, X'Pert PRO MPD, PANalytical, Netherland). To analyze the magnetic property of Fe_3O_4, a vibrating sample magnetometer (VSM, LakeShore Cryotronics, USA) was used.

2.5. Experimental design using the Box–Behnken

RSM has been widely used for optimizing the removal process and analyzing experimental results. Also, besides RSM can effectively evaluate the interaction of several parameters and provide an optimal response with the least number of designed experiments [25–29].

In this article, we used Design Expert 11 Software (Stat-Ease Inc.) for optimization of the turbidity removal based on the BBD to reach the maximum efficiency of turbidity removal as the response, which is a function of independent variables such as pH (4–9), mixing time in the rapid mixing unit (2–60 s), and $FeCl_3$ concentration (5–80 mg/L). The value ranges were assigned to effective parameters based on the pretests. The parameters labeled as A, B, and C were varied over three levels (–1, 0, +1) as shown in Table 1.

According to the software output, 17 experiments were designed based on BBD (Table 2). The central point (0,0,0) was repeated 5 times to evaluate the error in the results. The significance coefficient of the model was determined by the *p*-value. If the *p*-value is less than 0.05, the response variables are significant.

2.6. Mathematical modeling and regression analysis

Five models, which are mean, linear, 2FI, quadratic, and cubic were tested by the software. In the quadratic

Table 1
Experimental levels and ranges of effective parameters

Factor	Name	Coded level		
		–1	0	1
A	pH	4	6.5	9
B	$FeCl_3$, mg/L	5	42.5	80
C	Mixing time*, s	2	31	60

*Mixing time in the rapid mixing unit

Table 2
Design matrix for turbidity removal efficiency

Std	Run	*A*	*B*	*C*	Turbidity removal (%)	
		pH	$FeCl_3$ (mg/L)	Mixing time (s)	Actual	Predicted
1	2	4	5	31	79.06	80.30
2	1	9	5	31	80.63	78.60
3	16	4	80	31	71.2	77.62
4	7	9	80	31	94.76	91.56
5	3	4	42.5	2	78.01	94.14
6	14	9	42.5	2	89.53	86.71
7	13	4	42.5	60	78.01	95.22
8	9	9	42.5	60	92.15	94.14
9	6	6.5	5	2	85.86	92.54
10	15	6.5	80	2	93.19	94.14
11	4	6.5	5	60	91.62	92.87
12	11	6.5	80	60	93.72	94.14
13	17	6.5	42.5	31	92.67	78.53
14	10	6.5	42.5	31	95.29	89.01b
15	5	6.5	42.5	31	93.19	93.25
16	8	6.5	42.5	31	95.29	71.53
17	12	6.5	42.5	31	94.24	94.14

equation, the predicted response (turbidity removal efficiency) is expressed as the function of variables as follows:

$$Y_m = b_0 + \sum_{i=1}^{k} b_i x_i + \sum_{i=1}^{k} b_{ii} x_i^2 + \sum_{i}^{i<j} \sum_{j} b_{ij} x_i x_j \quad (1)$$

where Y_m is the response value (turbidity removal efficiency), x_i and x_j represent independent variables, b_0 is the constant term, b_i, b_{ii}, and b_{ij} represent coefficients of linear effect, squared effect, and the interaction effect, respectively. Analysis of variance (ANOVA), the sum of squares (R^2), and the adjusted sum of squares (Adj. R^2) were used to analyze the data and quality of the model [30,31].

2.7. Analytical methods

All experiments were conducted based on standard methods. The experiments were replicated twice, and the average of two measurements was reported [32]. Coagulation–flocculation experiments were performed using a standard Jar Tester (Co., Aqualytic). In this study, the pH and turbidity were measured using Metrohm 610 pH-Meter and Hach 2100 N turbidimeter, respectively. The turbidity removal efficiency (TRE) was calculated using Eq. (2)

$$\mathrm{TRE}(\%) = \frac{T_0 - T}{T_0} \times 100 \quad (2)$$

where T_0 and T are the initial and final turbidity (NTU), respectively.

3. Results and discussion

3.1. Structural characterization of Fe_3O_4 and GO

The SEM image in Fig. 1a shows that the dimension of smooth layers of GO nanosheets is approximately between 1–5 micrometers. On the other hand, Fig. 1b is related to the

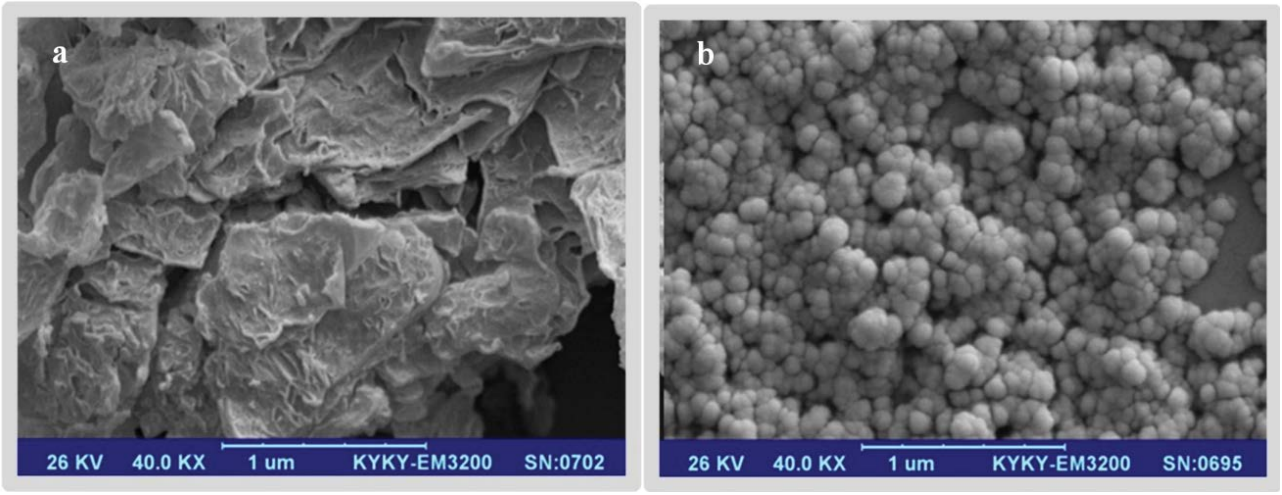

Fig. 1. SEM images of (a) GO and (b) Fe_3O_4.

SEM of Fe_3O_4 nanoparticles. As can be seen, the particles are spherical with a particle size of about 50 nm.

The XRD spectrum of Fe_3O_4 is shown in Fig. 2a. It can be recognized that all peaks are very broad, revealing the small crystal size of particles and homogeneity of the sample that was similar to crystal planes of a pure Fe_3O_4 with a spinal structure.

According to Fig. 2b, the magnetization of the Fe_3O_4 nanoparticles at 25°C vs. magnetic field, the saturation magnetization of Fe_3O_4 nanoparticles was almost 40 emu/g, showing the magnetic nature of Fe_3O_4, which is necessary to separate magnetic coagulant.

3.2. Statistical analysis of the response models

For turbidity removal efficiency, the quadratic model [Eq. (3)] was selected as it has the highest order polynomial with a significant sum of squares, insignificant lack-of-fit, and the highest R^2.

$$Y_{\text{turbidity removal}} = 21.19082 + 19.93907A - 0.10868B + 0.031737C + 0.058640AB + 9.03448\times10^{-3}AC - 1.2023\times10^{-3}BC - 1.55168A^2 - 2.15147\times10^{-3}B^2 - 1.54578\times10^{-5}C^2 \quad (3)$$

In this equation, A, B, C, and Y are the pH, $FeCl_3$, mixing time, and predicted turbidity removal efficiency, respectively. The positive and negative signs in front of the terms indicate the synergistic and antagonistic effect respectively. The R^2 value of 0.9909 was a good indicator, showing that a high proportion of variability (up to 99%) was explained by the data. ANOVA for the response surface quadratic model was conducted to obtain the significance level of the fitted model and the factors affecting the turbidity removal efficiency. ANOVA for the quadratic model is illustrated in Table 3.

The model F-value of 84.50 and p-value less than 0.050 indicate that the model and model terms are significant.

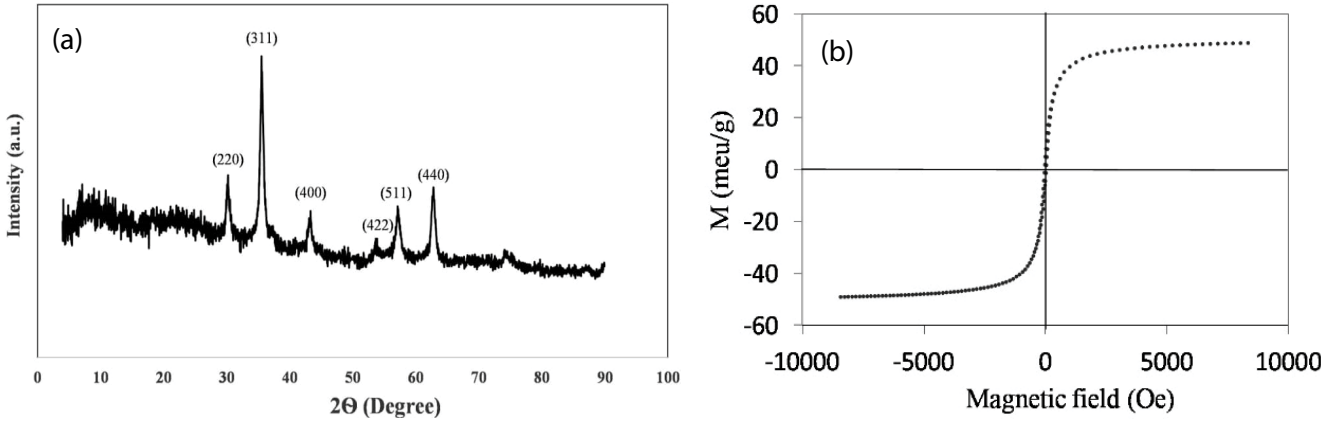

Fig. 2. (a) XRD pattern of Fe_3O_4 and (b) VSM graph for Fe_3O_4.

Table 3
ANOVA for the response surface quadratic model for turbidity removal efficiency

Source	Sum of squares	df	Mean square	F-value	p-value Prob. > F	
Model	943.62	9	104.85	84.50	<0.0001	significant
A-pH	322.45	1	322.45	259.89	<0.0001	
B-$FeCl_3$	30.81	1	30.81	24.83	0.0016	
C-Mixing time	9.92	1	9.92	8.00	0.0255	
AB	120.89	1	120.89	97.43	<0.0001	
AC	1.72	1	1.72	1.38	0.2780	
BC	6.84	1	6.84	5.51	0.0513	
A^2	396.01	1	396.01	319.17	<0.0001	
B^2	38.54	1	38.54	31.06	0.0008	
C^2	7.116E-004	1	7.116E-004	5.735E-004	0.9816	
Residual	8.69	7	1.24			
Lack of fit	2.97	3	0.99	0.69	0.6032	not significant
Pure error	5.72	4	1.43			
Cor. total	952.31	16				

R^2 = 0.9909; Adj. R^2 = 0.9792; Pred. R^2 = 0.9408; C.V. = 1.26%; Adeq. Precision = 27.77

Also, there is only a 0.01% chance that such a large *F*-value could occur due to noise. Herein, *A*, *B*, *C*, *AB*, A^2, and B^2 are significant model terms. The values greater than 0.10 imply that the model terms are not significant. If there are many insignificant model terms, model reduction may improve the model. In this case, only *AC* and C^2 are not significant model terms. There is a 60.32% chance that such a large lack of fit "*F*-value" could occur due to noise. According to Table 3, the high R^2-values determine the appropriate agreement between the calculated and experimental data. Also, the difference between the predicted determination coefficients (Pred. R^2 of 0.9408) and the adjusted determination coefficient (Adj. R^2 of 0.9792) was less than 0.2, which proved the accuracy of the model. Additionally, Adeq. Precision, specifying the signal-to-noise ratio, was greater than 4, indicating an adequate signal [33].

The pareto graph in Fig. 3 indicates the effect of independent parameters in turbidity removal. According to Fig. 3, pH × pH and pH parameters have the most impact on turbidity removal, respectively. The high effect of pH parameter on turbidity removal can be due to hydrolysis of $FeCl_3$ to $Fe(OH)_2^+$, $Fe(OH)_3$, and $Fe(OH)_2^+$ at pH below 8 [34].

The predicted values of turbidity removal efficiency were plotted vs. the actual values, as shown in Fig. 4. The predicted points have almost linear behavior and show that they agree with the experimental data.

3.3. Three-dimensional model and contour of regression models

The three-dimensional (3D) response surface plots and relevant contour plots are very effective for showing the effect of the independent variables on the responses. We can investigate the effect of independent variables on the response at different points by examining graphical shapes. In this way, by finding the intersection point between the variables, it is possible to find and record the exact amount of the measured parameter [35]. To investigate these charts, two independent variables and one dependent

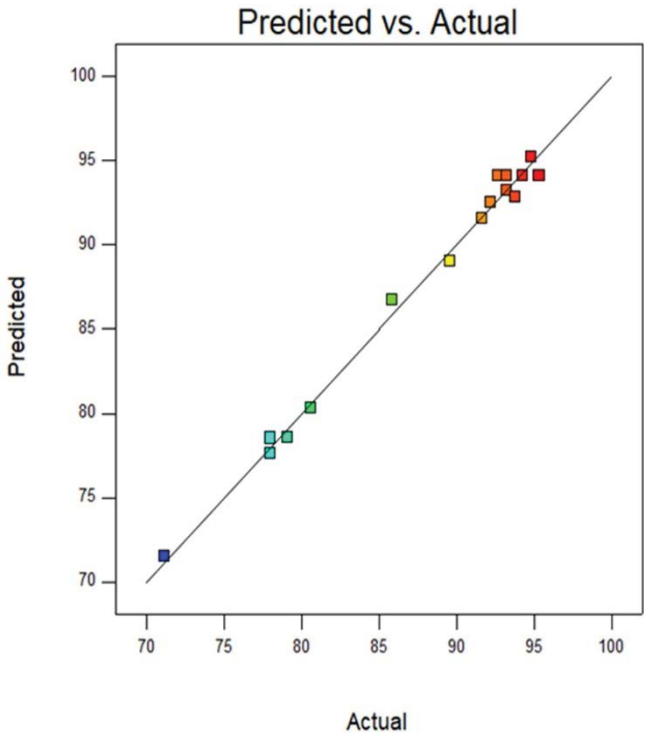

Fig. 4. Comparison between the actual and predicted values for turbidity removal efficiency.

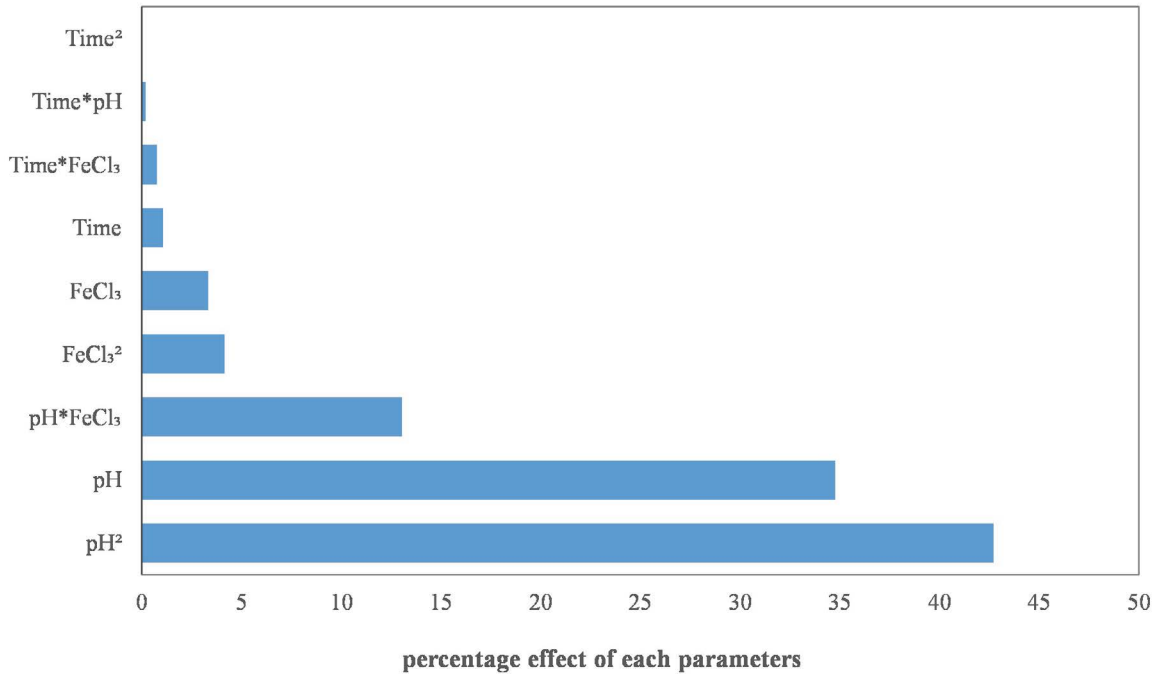

Fig. 3. Pareto graph of the conventional CFP for the effect of each parameter.

variable were plotted. In contrast, the third independent variable was kept constant in its central value (the mean value provided by the software with maximum and minimum values). The three-dimensional models and contour regression models are shown in Fig. 5.

Fig. 5a and b represent the interaction of pH with $FeCl_3$ concentration when mixing time is at the center point of 31 min. Fig. 5a shows a nonlinear curved surface and the results show that both pH and $FeCl_3$ dosage affect turbidity removal efficiency. Fig. 5c and d show the interaction of pH and mixing time when the $FeCl_3$ dosage is at the center point of 42.5 mg/L. As can be seen, the effect of pH on turbidity removal is more than that of mixing time. Fig. 5e and f show the interaction of mixing time with $FeCl_3$ dosage when pH is at the center point of 6.5. The three-dimensional and contour regression models show that the interaction of the two parameters is negligible.

3.4. Effect of independent variables on the response

The impact of each independent variable on the efficiency of turbidity removal, illustrated in Fig. 6, was explained separately. As it is shown, pH is more efficacious than $FeCl_3$ dosage and mixing time.

3.4.1. Effect of pH on the turbidity removal

The removal of turbidity can be attributed to species derived from $FeCl_3$ hydrolysis. When $FeCl_3$ is added to aqueous solutions, it is hydrolyzed at pH below 8 to $Fe(OH)_2^+$, $Fe(OH)_3$, and $Fe(OH)_2^+$. The most common spices in the pH range of 5 to 8 are $Fe(OH)_2^+$ and $Fe(OH)_3$ [34]. The three-dimensional model in Fig. 5a and the contour of the regression model in Fig. 5b show that pH plays a significant role in turbidity removal efficiency. By increasing pH, the efficiency of turbidity removal goes up. Also, Fig. 6 is noticed that the effect of pH on the reduction of turbidity is higher than that of the other two parameters, consistent with the results reported by Neamati et al. [36]. The optimal pH range of 7.0–7.5 has been reported by Pirsaheb et al. [37] for $FeCl_3$ to eliminate turbidity. The impact of pH on turbidity removal was examined by Ramavandi [38], which concluded when the pH rises from 2 to 6, the efficiency of turbidity removal elevates from 97% to 99.6%. Furthermore, the elimination of antimony by the use of $FeCl_3$ and poly aluminum chloride coagulants was investigated by Kang et al. [39]. They found that pH effectively influences the elimination of antimony by $FeCl_3$. In this study, the efficiency of turbidity removal was high at pH–6.5.

According to the reported researches, ZPC for zeolite is 4. This means that at pH below 4, the charge of zeolite is positive, and at pH above 4, its charge becomes negative [40,41]. Therefore, at pH 6.5, the zeolite has a negative charge and the hydrolyzed species of coagulant $Fe(OH)_2^+$ and $Fe(OH)^{2+}$ have positive charge, resulting in neutralization of the surface charge of zeolite particles. Therefore, aggregating and subsequent settling occurs. As a result, the highest efficiency of turbidity removal occurs at pH = 6.5. However, electrostatic repulsion occurs when pH is higher than 6.5 because $Fe(OH)_4^-$ is the predominant ionic species derived from the coagulant, and zeolite particles have a negative charge. Thus, the particles are not able to settle, thereby reducing the efficiency of turbidity.

3.4.2. Effect of $FeCl_3$ dosage on the efficiency of turbidity removal

A large number of $Fe(OH)_2^+$ and $Fe(OH)_3$ species have been produced by increasing the amount of $FeCl_3$ coagulant. An investigation conducted by Nemati et al. showed that the rate of color and turbidity removal was the highest at pH = 6.2 and 40 mg/L of $FeCl_3$ [36]. According to the three-dimensional model presented in Fig. 5a and the contour of the regression model depicted in Fig. 5b, the changes in $FeCl_3$ affected the efficiency of turbidity removal. When the $FeCl_3$ dosage increased, the efficiency of turbidity removal increased. As shown in Fig. 6, the effect of $FeCl_3$ dosage was less than that of pH and more than that of the mixing time.

Ebeling et al. showed that 90 mg/L of alum and $FeCl_3$ was sufficient in removing suspended solids in the range of 10 to 100 mg/L [42]. In another study conducted by Hesami et al. at pH = 5, the optimized $FeCl_3$ dosage for removing turbidity was 10 mg/L. The results showed that by increasing the $FeCl_3$ dose, the amount of residual turbidity decreased due to the increase in particle accumulation and the formation of more flocs [43]. Baghvand et al. examined the optimization of the CFP using iron and aluminum salts for water in the turbidity range of 10–1,000 NTU. The results showed that 10–20 mg/L of coagulant was the best dose for turbidity removal [44]. In this investigation, according to the concentrations considered for $FeCl_3$, as well as the three-dimensional model, the efficiency of turbidity removal at concentrations greater than 40 mg/L was higher than 95%, which can be due to the increase in $Fe(OH)_3$ and consequently an increase in separation of turbidity at pH above 4.

3.4.3. Effect of mixing time in the rapid mixing unit on turbidity removal

The three-dimensional graph in Fig. 5c and e shows that the mixing time has no significant impact on the efficiency of turbidity removal, but enhancing the level of pH is important to increase the efficiency of turbidity removal. Also, according to Fig. 6, the effect of the mixing time in the rapid mixing unit on the reduction of turbidity was less than that of the other two parameters.

3.5. Optimization of parameters and confirmation of results

To find the optimal point, five goals are provided by the software, which is maximize, minimize, target, in range, and equal to. Since this study aims to maximize the turbidity removal efficiency, the goal "in range" was selected for the independent variables, and "maximize" goals were chosen for the response. Then, the optimization program was performed by the software, the result of which is given in Table 4. According to the optimum conditions, the maximum turbidity removal was 95.75%, which was achieved

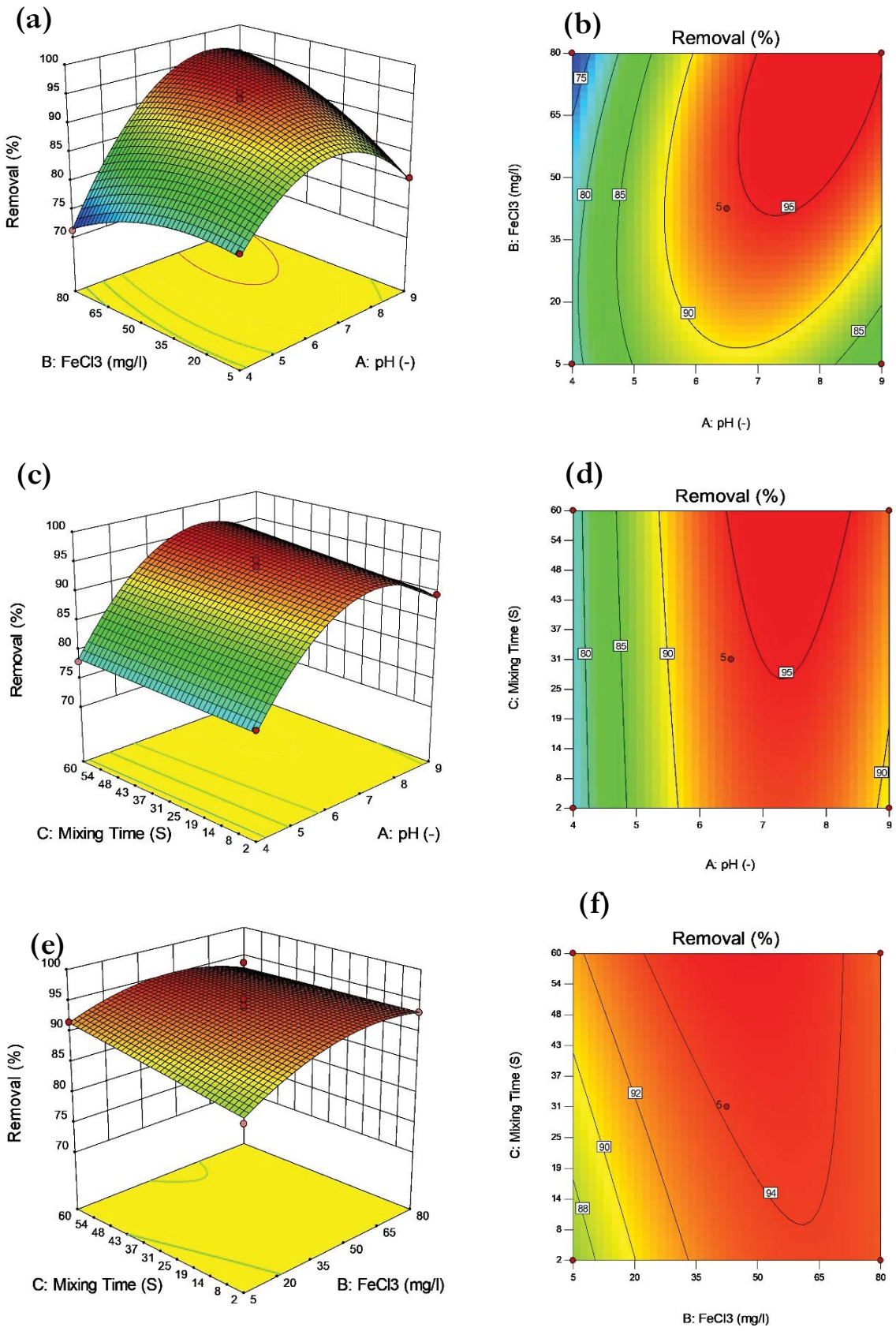

Fig. 5. Three-dimensional and contour of regression models for turbidity removal: (a, b) effect of pH and $FeCl_3$ dosage, (c,d) effect of pH and mixing time, and (e,f) effect of $FeCl_3$ dosage and mixing time.

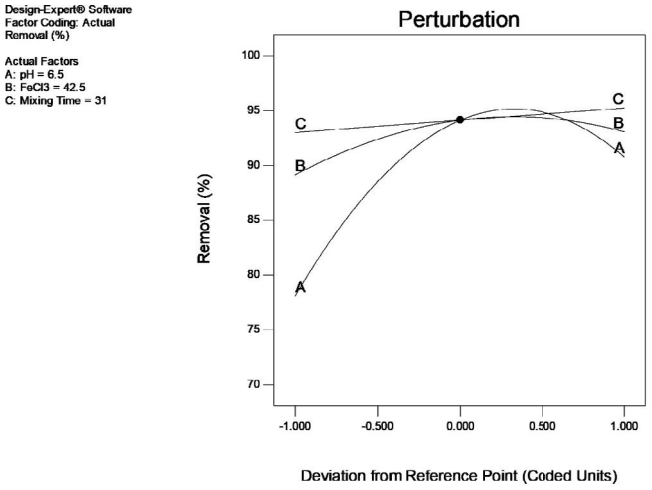

Fig. 6. Effect of independent variables on the turbidity removal.

Table 4
Parameters for numerical optimization

pH	6.9
$FeCl_3$	48
Mixing time	46
Removal	95.75
Desirability	1.000
	Selected

at pH 6.9, 48 mg/L of $FeCl_3$, and 46 s for mixing time in the rapid mixing unit. The minimum effluent turbidity was 8 NTU; therefore, To meet the Iranian drinking water standard, the turbidity has to be decline less than 5 NTU. For this purpose, the effluent of the coagulation-flocculation after the settling unit should be transferred to the filtration unit.

In order to confirm the results of the optimized parameters, three steps of the Jar-Test experiment were performed based on the optimal operating conditions. According to the results presented in Table 5, the average turbidity removal was 95.4%, which was in the 95% confidence interval, confirming the accuracy of the optimization results.

3.6. Effect of graphene oxide and Fe_3O_4 on turbidity removal

After determining the optimal operating conditions with the design expert software, the performance of graphene oxide and the combination of graphene oxide and Fe_3O_4 were examined to evaluate the efficiency of turbidity removal. In this study, firstly, graphene oxide and $FeCl_3$ were added to synthesized water according 2.3 section. The ZPC of graphene oxide is 3–4, so at the neutral pH, the graphene oxide charge becomes negative. On the other hand, the zeolite charge is also negative. The settling time of the flocs, in this case, increased compared to normal coagulation conditions, which was about 60 min. In this investigation, the turbidity was 10 NTU and the efficiency of turbidity removal was 94.7%, which is compatible with the results of Aboubaraka [20]. As a matter of fact that the formed flocs were small and did not settle well, in the next step, Fe_3O_4 was added to $FeCl_3$ and graphene oxide. As shown in Fig. 7, the formation of magnetic flocs led to removing flocs faster by applying a magnetic field and increasing the settling speed of the flocs. In this study, not only did the flocs condense, but also the settling time decreased from 30 min to about 1 min [45].

Table 5
Confirmation results for optimized parameters

Response	Removal
Mean	95.7
Median	95.75
Observed	–
Std. Dev.	1.113
n	3
SE pred.	0.81
95% PI low	93.83
Data mean	95.4
95% PI high	97.7

3.7. Comparison of conventional and modified CFP on the turbidity removal

The effluent turbidity, settling time of flocs and chemical material cost were compared to conventional and modified (GO + $FeCl_3$ and GO + Fe_3O_4 + $FeCl_3$) CFP.

As shown in Fig. 8, the lowest level of turbidity and settling time in treated water was observed in the modified CFP (GO + Fe_3O_4 + $FeCl_3$). According to Fig. 8, for providing the turbidity of less than 5 NTU, the calculated costs of chemical materials is 2 \$/m^3 for modified CFP (GO + Fe_3O_4 + $FeCl_3$). Although the lowest cost of chemical materials is for the conventional CFP (0.5 \$/m^3), but effluent turbidity will not be provided according to the existing standards. The research conducted by Kalavathy et al. [11] confirmed this subject. Therefore, not only is a sedimentation tank with settling time of more than 30 min required but also gravity or pressure filtration (sand or sand + anthracite stages) should be used after sedimentation to meet the standard. However, filtration has high operating costs because of filter clogging, backwash pump, air blower, replacement of sand and anthracite, piping, etc. Consequently, magnetic separation can be used instead of sedimentation tank and filtration due to the low settling time (about 1 min) and the simple separation of magnetic nanoparticles by using an external magnetic field. This method has advantages such as less sludge production, higher efficiency, reduced operating problems, reduced settling time, and so on.

Table 6 compares some of the published literature on turbidity removal by different coagulants with the results of this study. According to Table 6 the turbidity removal efficiency in the modified CFP with graphene oxide (GO) and magnetic (Fe_3O_4) nanoparticles in this study was higher than articles with similar turbidity and provided the turbidity of less than 5 NTU.

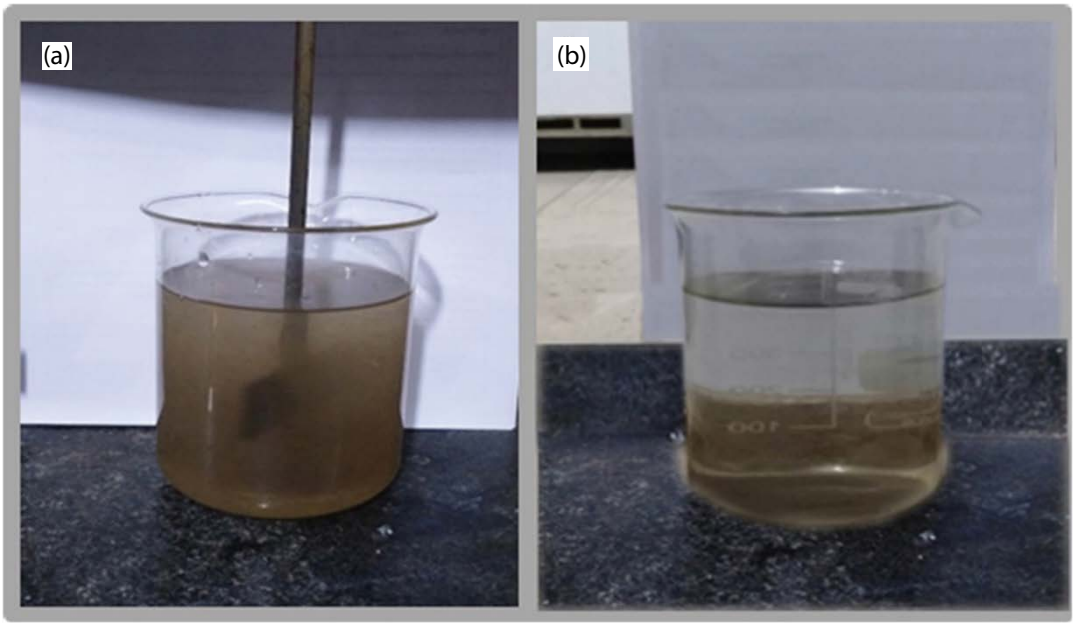

Fig. 7. (a) Flocs formed and (b) flocs deposited at pH = 6.5, $FeCl_3$ coagulant, GO (10 mg/L) and Fe_3O_4 (4 mg/L).

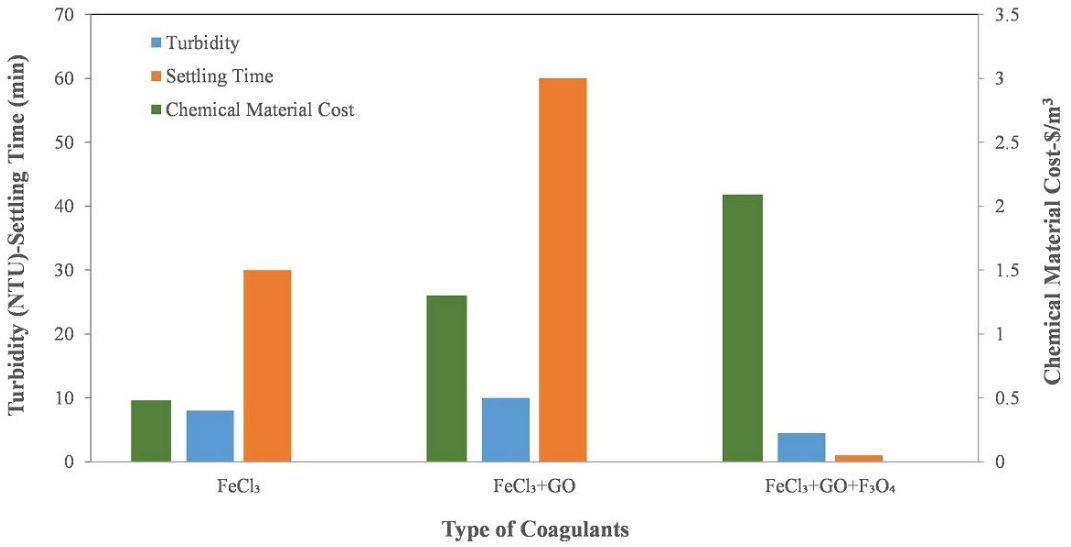

Fig. 8. Comparison of conventional and modified CFP on the turbidity removal.

Table 6
Comparison of recently published literatures and this study on turbidity removal efficiency

Coagulants	Initial turbidity	Turbidity type	Turbidity removal efficiency (%)	References
PACL + Fe_3O_4 + PAM	20–100 NTU	Kaoline	89.75–96.80	[18]
GO + Fe_3O_4 + $FeCl_3$	180 FTU	Humic acid	95.3	[19]
$FeCl_3$	80 NTU	Bentonite	71–80	[11]
GO	20–200 NTU	Kaoline	<95	[20]
GO + PAC	–	Kaoline + Humic acid	<80	[13]
$FeCl_3$	191 NTU	Zeolite	95.7	This study
GO + $FeCl_3$	191 NTU	Zeolite	94.7	This study
GO + Fe_3O_4 + $FeCl_3$	191 NTU	Zeolite	97.6	This study

4. Conclusions

Conventional and modified CFP were used for turbidity removal from synthetic water. BBD and RSM were applied for Conventional CFP modeling and optimization. Among the parameters, pH had the most significant effect on the reduction of turbidity. The optimum conditions of pH, $FeCl_3$, and the mixing time in the rapid mixing unit were 6.9, 48 mg/L, and 46 s, respectively, for the turbidity reduction to 8 NTU. The maximum turbidity removal efficiency with GO + $FeCl_3$ and GO + Fe_3O_4 + $FeCl_3$ were 94.7% and 97.6%, respectively. Furthermore, settling time decreased from 30 min to 1 min under the optimal conditions when GO and Fe_3O_4 were utilized simultaneously. In these conditions, the residual turbidity was less than 5 NTU.

Declaration of competing interest

This research did not receive any specific grant from funding agencies in the public, commercial, or not-for-profit sectors.

Acknowledgments

The authors willingly recognize the Nanotechnology Research Center of School of Environment, College of Engineering, University of Tehran.

References

[1] B. Feizizadeh, Z. Ronagh, S. Pourmoradian, H.A. Gheshlaghi, T. Lakes, T. Blaschke, An efficient GIS-based approach for sustainability assessment of urban drinking water consumption patterns: a study in Tabriz city, Iran, Sustainable Cities Soc., 64 (2021) 102584, doi: 10.1016/j.scs.2020.102584.
[2] P. Beaudeau, A systematic review of the time series studies addressing the endemic risk of acute gastroenteritis according to drinking water operation conditions in urban areas of developed countries, Int. J. Environ. Res. Public Health, 15 (2018) 867, doi: 10.3390/ijerph15050867.
[3] R. Muoio, C. Caretti, L. Rossi, D. Santianni, C. Lubello, Water safety plans and risk assessment: a novel procedure applied to treated water turbidity and gastrointestinal diseases, Int. J. Hyg. Environ. Health, 223 (2020) 281–288.
[4] S. Shahvi, A. Torabian, Studying iranian drinking water quality guidelines compared to the authentic world standards, J. Water Wastewater Sci. Eng., 2 (2017) 3–13.
[5] S. Ghafari, H.A. Aziz, M.H. Isa, A.A. Zinatizadeh, Application of response surface methodology (RSM) to optimize coagulation–flocculation treatment of leachate using poly-aluminum chloride (PAC) and alum, J. Hazard. Mater., 163 (2009) 650–656.
[6] Y. Sun, S. Zhou, P.C. Chiang, K.J. Shah, Evaluation and optimization of enhanced coagulation process: water-energy nexus, Water-Energy Nexus, 2 (2020) 25–36.
[7] M.G. Antov, M.B. Šćiban, J.M. Prodanović, Evaluation of the efficiency of natural coagulant obtained by ultrafiltration of common bean seed extract in water turbidity removal, Ecol. Eng., 49 (2012) 48–52.
[8] M. Racar, D. Dolar, A. Špehar, A. Kraš, K. Košutić, Optimization of coagulation with ferric chloride as a pretreatment for fouling reduction during nanofiltration of rendering plant secondary effluent, Chemosphere, 181 (2017) 485–491.
[9] L.C.M. Tavares, A.C. Borges, T.C.F. da Silva, A.P. Rosa, Guazuma ulmifolia: an environmentally friendly coagulant aid for water treatment, Water Sci. Technol., 82 (2020) 1579–1585.
[10] J.M. Thamer, S. Eman, Effect of settling time, velocity gradient, and camp number on turbidity removal for oilfield produced water, Egypt. J. Pet., 27 (2018) 31–36.
[11] S. Kalavathy, M. Giridhar, G. Viswanadh, A Jar Test Study on the use of Alum and Ferric Chloride for Turbidity Removal, Proceedings of 4th National Conference on Water, Environment & Society, Hyderabad, India, 2017.
[12] S. Usefi, M.A. Ghalhari, Modeling and optimization of the coagulation–flocculation process in turbidity removal from aqueous solutions using rice starch, Pollution, 5 (2019) 623–636.
[13] Z. Yang, H. Yan, H. Yang, H. Li, A. Li, R. Cheng, Flocculation performance and mechanism of graphene oxide for removal of various contaminants from water, Water Res., 47 (2013) 3037–3046.
[14] S.R. Kanel, H. Misak, D. Nepal, S. Mall, S.W. Brittle, I. Sizemore, D.M. Kempisty, M.N. Goltz, The use of carbon nanotube yarn as a filter medium to treat nitroaromatic-contaminated water, New Carbon Mater., 31 (2016) 415–423.
[15] A. Azari, R. Nabizadeh, S. Nasseri, A.H. Mahvi, A.R. Mesdaghinia, Comprehensive systematic review and meta-analysis of dyes adsorption by carbon-based adsorbent materials: classification and analysis of last decade studies, Chemosphere, 250 (2020) 126238, doi: 10.1016/j.chemosphere.2020.126238.
[16] A. Azari, A.A. Babaie, R.R. Kalantary, A. Esrafili, M. Moazzen, B. Kakavandi, Nitrate removal from aqueous solution by carbon nanotubes magnetized with nano zero-valent iron, J. Mazandaran Univ. Med. Sci., 23 (2014) 15–27.
[17] R.R. Kalantary, A.J. Jafari, B. Kakavandi, S. Nasseri, A. Ameri, A. Azari, Adsorption and magnetic separation of lead from synthetic wastewater using carbon/iron oxide nanoparticles composite, J. Mazandaran Univ. Med. Sci., 24 (2014) 172–183.
[18] M. Lv, Z. Zhang, J. Zeng, J. Liu, M. Sun, R.S. Yadav, Y. Feng, Roles of magnetic particles in magnetic seeding coagulation–flocculation process for surface water treatment, Sep. Purif. Technol., 212 (2019) 337–343.
[19] M.M. Parsa, H. Pourfakhar, M. Baghdadi, Application of graphene oxide nanosheets in the coagulation–flocculation process for removal of Total Organic Carbon (TOC) from surface water, J. Water Process Eng., 37 (2020) 101367, doi: 10.1016/j.jwpe.2020.101367.
[20] A.E. Aboubaraka, E.F. Aboelfetoh, E.Z.M. Ebeid, Coagulation effectiveness of graphene oxide for the removal of turbidity from raw surface water, Chemosphere, 181 (2017) 738–746.
[21] R.D. Ambashta, M. Sillanpää, Water purification using magnetic assistance: a review, J. Hazard. Mater., 180 (2010) 38–49.
[22] X. Yang, C. Chen, J. Li, G. Zhao, X. Ren, X. Wang, Graphene oxide-iron oxide and reduced graphene oxide-iron oxide hybrid materials for the removal of organic and inorganic pollutants, RSC Adv., 2 (2012) 8821–8826.
[23] S.M. Ghasemabadi, M. Baghdadi, E. Safari, F. Ghazban, Investigation of continuous adsorption of Pb(II), As(III), Cd(II), and Cr(VI) using a mixture of magnetic graphite oxide and sand as a medium in a fixed-bed column, J. Environ. Chem. Eng., 6 (2018) 4840–4849.
[24] M. Baghdadi, E. Ghaffari, B. Aminzadeh, Removal of carbamazepine from municipal wastewater effluent using optimally synthesized magnetic activated carbon: adsorption and sedimentation kinetic studies, J. Environ. Chem. Eng., 4 (2016) 3309–3321.
[25] E. Hamed, A. Sakr, Application of multiple response optimization technique to extended release formulations design, J. Controlled Release, 73 (2001) 329–338.
[26] M.A. Bezerra, R.E. Santelli, E.P. Oliveira, L.S. Villar, L.A. Escaleira, Response surface methodology (RSM) as a tool for optimization in analytical chemistry, Talanta, 76 (2008) 965–977.
[27] A. Karami, K. Karimyan, R. Davoodi, M. Karimaei, K. Sharafie, S. Rahimi, T. Khosravi, M. Miri, H. Sharafi, A. Azari, Application of response surface methodology for statistical analysis, modeling, and optimization of malachite green removal from aqueous solutions by manganese-modified pumice adsorbent, Desal. Water Treat., 89 (2017) 150–161.
[28] S. Sharifi, R .Nabizadeh, B. Akbarpour, A. Azari, H.R. Ghaffari, S. Nazmara, B. Mahmoudi, L. Shiri, M. Yousefi, Modeling and optimizing parameters affecting hexavalent chromium adsorption from aqueous solutions using Ti-XAD7

nanocomposite: RSM-CCD approach, kinetic, and isotherm studies, J. Environ. Health Sci. Eng., 17 (2019) 873–888.
[29] A. Azari, M. Noorisepehr, E. Dehghanifard, K. Karimyan, S.Y. Hashemi, E.M. Kalhori, R. Norouzi, S. Agarwal, V.K. Gupta, Experimental design, modeling and mechanism of cationic dyes biosorption on to magnetic chitosan-lutaraldehyde composite, Int. J. Biol. Macromol., 131 (2019) 633–645.
[30] Y. Nazir, S. Shuib, M.S. Kalil, Y. Song, A.A. Hamid, Optimization of culture conditions for enhanced growth, lipid and docosahexaenoic acid (DHA) production of *Aurantiochytrium* SW1 by response surface methodology, Sci. Rep., 8 (2018) 1–12.
[31] M. Nourani, M. Baghdadi, M. Javan, G.N. Bidhendi, Production of a biodegradable flocculant from cotton and evaluation of its performance in coagulation–flocculation of kaolin clay suspension: optimization through response surface methodology (RSM), J. Environ. Chem. Eng., 4 (2016) 1996–2003.
[32] R.B. Baird, A.D. Eaton, E.W. Rice, Standard Methods for the Examination of Water and Wastewater, Water Environment Federation, American Public Health Association, America, 2017.
[33] D.C. Montgomery, Design and Analysis of Experiments, John Wiley & Sons, Arizona State University, 2017.
[34] J. Gregory, J. Duan, Hydrolyzing metal salts as coagulants, Pure Appl. Chem., 73 (2001) 2017–2026.
[35] S.M.T. Gharibzahedi, S.M. Mousavi, M. Hamedi, M. Ghasemlou, Response surface modeling for optimization of formulation variables and physical stability assessment of walnut oil-in-water beverage emulsions, Food Hydrocolloids, 26 (2012) 293–301.
[36] B. Neamati, M. Sadeghi, A. Fadaei, M. Sedehi, M. Azari, T. Mohamadi, removal of color and turbidity of waters containing natural organic materials using integrated enhanced coagulation and direct filtration, J. Shahrekord Univ. Med. Sci., 18 (2016) 122–131.
[37] M. Pirsaheb, A.A. Zinatizadeh, A. Dargahi, Performance evaluation of coagulation process in removal of low turbidity and color from water using different inorganic coagulants, J Water Wastewater, 23 (2012) 111–118.
[38] B. Ramavandi, Treatment of water turbidity and bacteria by using a coagulant extracted from *Plantago ovata*, Water Resour. Ind., 6 (2014) 36–50.
[39] M. Kang, T. Kamei, Y. Magara, Comparing polyaluminum chloride and ferric chloride for antimony removal, Water Res., 37 (2003) 4171–4179.
[40] T. Kuzniatsova, Y. Kim, K. Shqau, P.K. Dutta, H. Verweij, Zeta potential measurements of zeolite Y: application in homogeneous deposition of particle coatings, Microporous Mesoporous Mater., 103 (2007) 102–107.
[41] X. Liu, P.M. Arvela, A. Aho, Z. Vajglova, V.M. Gun'ko, I. Heinmaa, N. Kumar, K. Eränen, T. Salmi, D.Y. Murzin, Zeta potential of beta zeolites: influence of structure, acidity, pH, temperature and concentration, Molecules, 23 (2018) 946, doi: 10.3390/molecules23040946.
[42] J.M. Ebeling, P.L. Sibrell, S.R. Ogden, S.T. Summerfelt, Evaluation of chemical coagulation–flocculation aids for the removal of suspended solids and phosphorus from intensive recirculating aquaculture effluent discharge, Aquacult. Eng., 29 (2003) 23–42.
[43] F. Hesami, B. Bina, A. Ebrahimi, The effectiveness of chitosan as coagulatin Aid in turbidity removal from water, Int. J. Environ. Health Eng., 3 (2014) 46–51.
[44] A. Baghvand, A.D. Zand, N. Mehrdadi, A. Karbassi, Optimizing coagulation process for low to high turbidity waters using aluminum and iron salts, Am. J. Environ. Sci., 6 (2010) 442–448.
[45] S.L. Lo, Y.L. Wang, C.Y. Hu, High turbidity reduction durin the storm period by applied magnetic field, J. Environ. Eng. Manage., 17 (2007) 365–370.